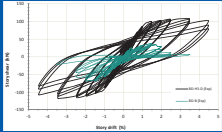
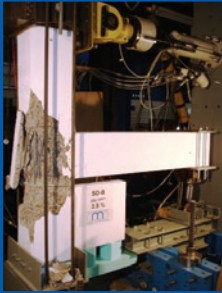




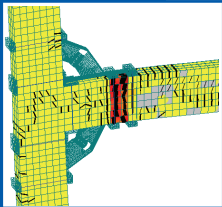
Berichte des Instituts für Massivbau



Mahdi Hayatrouhi



Strengthening of reinforced concrete beam-column joints to increase seismic resistance



Berichte

des Instituts für Massivbau der Leibniz Universität Hannover
Herausgeber:
Univ.-Prof. Dr.-Ing. Steffen Marx
Leibniz Universität Hannover – Institut für Massivbau
Heft 9, Februar 2014

Fraunhofer IRB Verlag

Herausgeber

Univ.-Prof. Dr.-Ing. Steffen Marx
Leibniz Universität Hannover
Institut für Massivbau
Appelstraße 9 A
30167 Hannover

Alle Rechte vorbehalten

Dieses Werk einschließlich aller seiner Teile ist urheberrechtlich geschützt. Jede Verwertung in anderen als den gesetzlich zugelassenen Fällen bedarf deshalb der vorherigen schriftlichen Einwilligung des Herausgebers.

© 2014 by Univ.-Prof. Steffen Marx
Leibniz Universität Hannover
Institut für Massivbau
ISBN (Print): 978-3-8167-9177-5
ISBN (E-Book): 978-3-8167-9178-2

Fraunhofer IRB Verlag

Fraunhofer-Informationszentrum Raum und Bau IRB
Postfach 80 04 60, 70504 Stuttgart
Telefon 0711 970-2500
Telefax 0711 970-2508
E-Mail irb@irb.fraunhofer.de
URL <http://www.baufachinformation.de>

Abstract

Current research attempted to explore the behaviour of critical regions of reinforced concrete frame structures under seismic loading to investigate the deficiencies and evaluate the performance of gravity load designed (GLD) reinforced concrete (RC) beam-column joints. The categorized literature review of retrofitting and strengthening methods of RC beam-column joints clarified that non-disruptiveness; practical implementation, ductility and perseverance of lateral resistance as well as economical issues still remain the most challenging aspects of seismically retrofitting the vulnerable existing RC beam-column joints.

The seismic design principals of RC frame structures were observed in seismic retrofitting of the vulnerable frames as a strategy of retrofitting based on the capacity design concept. Accordingly, the beam sidesway mechanism was redefined for seismic retrofitting by relocating the beam plastic hinges far enough away from the joints. Afterwards, with introducing innovative energy dissipation devices such as Multi Functional Corbels (HMFC) and Harmonica Damper Plates (HHDP), the innovative Retrofitting Techniques 1 and 2 (RT1 and RT2) were proposed. The introduced devices of HMFC and HHDP as a passive energy dissipation system absorb energy through inelastic deformations. For efficiently and extensively evaluating and arranging the anticipated hierarchy of strength in beam-column joints before and after retrofitting, the Strength and Failure Sequence Diagram (SFSD) was proposed in a new coordinate. To implement the proposed RT1 and RT2 and achieve the desired hierarchy of strength, the design procedures were presented. Subsequently, to clarify the behaviour and founding the proposed innovative devices and techniques a comprehensive numerical analysis was carried out by nonlinear finite element analysis software ATENA.

The proposed RT1 and RT2 were experimentally evaluated through a series of five 3/4-scale beam-column joint specimens including two units for reference and the three others for retrofitting. A particular loading setup was designed and fabricated in structural laboratory so that the applying of horizontal cyclic and vertical static loads became simultaneously possible. An extremely severe loading history including three cycles (push and pull) at every particular drift level as a displacement-controlled series of progressively increasing displacement amplitudes in accordance with [ACI 374.1-05] was imposed to every specimen. The excellent performance of retrofitted specimens through the experimental study confirmed that the proposed RT1 and RT2 are able to retain structural integrity with the minimum strength and

stiffness degradation. As intended, the energy dissipation capacity was dramatically increased and beam sidesway mechanism was actually formed.

Finally, non-linear finite element analysis using ATENA was carried out on all reference and retrofitted specimens. The FEM models were validated with experimental outcomes. Subsequently, the validated models were utilized to develop a new simplified method for upgrading based on the advantages of RT1 and RT2. In the new proposed innovative Retrofitting Technique 3 (RT3), HHDP was replaced by Frictional-Bending Damper Plate (HFBDP) which dissipates energy based on friction and bending. The effectiveness and reliability of the proposed RT3 was investigated through a numerical analysis. The results of simulation showed that RT3 could efficiently achieve the intention of seismic retrofitting too.

At the end, as confirmed through experimental and numerical investigation, it is claimed that the all acceptance criteria of ACI Committee 374 [ACI 374.1-05] were effectively satisfied by the proposed retrofitting techniques.

Keywords: beam-column joint; retrofitting; seismic; analysis; design; energy dissipation; plastic hinge; inelastic deformation; corbel; friction

Kurzzusammenfassung

Die Arbeit enthält eine kategorisierte Übersicht von Nachrüst- und Verstärkungsmethoden bewehrter Balken-Stützen-Verbindungen aus der Literatur. Es zeigt sich, dass sowohl baulicher Eingriff, praktische Ausführung, Duktilität und Dauerhaftigkeit bezüglich seitlichen Widerstands, als auch ökonomische Randbedingungen die herausforderndsten Aspekte seismischer Verstärkungen gefährdeter Balken-Stützen-Verbindungen aus Stahlbeton sind.

Die seismischen Konstruktionsprinzipien von Stahlbetonrahmenkonstruktionen wurden entsprechend der Strategie für Nachrüstungen nach dem „capacity design concept“ untersucht. Dabei wurde der „beam sidesway mechanism“ für seismische Verstärkungen durch eine Verlagerung des plastischen Gelenks in geeigneter Entfernung zur Rahmenecke neu definiert. Danach werden durch Einführung innovativer Energiedissipationsgeräte, wie Multifunktionskonsole (HMFC) und Harmonika-Dämpfer-Platte (HHDP), innovative Verstärkungstechniken 1 und 2 (RT1 und RT2) vorgeschlagen. Die innovativen Geräte HMFC und HHDP als passives Energiedissipationssystem absorbieren Energie durch unelastische Verformung. Zur effizienten und ausgedehnten Bewertung und Anordnung erwarteter Widerstandshierarchie in Balken-Stützen-Verbindungen vor und nach der Verstärkung, wurde das Widerstands-Versagensfolge-Diagramm (SFSD) mit veränderter Ordinate vorgeschlagen. Zur Anwendung der eingeführten RT1 und RT2 und zum Erreichen der gewünschten Widerstandshierarchie wurde ein kompletter Entwurfsprozess präsentiert. Um das Verhalten und die Leistungsfähigkeit des vorgeschlagenen innovativen Geräts und Techniken zu untermauern, wurden umfassende numerische Analysen mit der nichtlinearen FE-Software ATENA durchgeführt.

Die vorgeschlagenen Verstärkungstechniken wurden experimentell mittels einer Serie von 5 Balken-Stützen-Verbindungen im $\frac{3}{4}$ -Maßstab evaluiert, wobei zwei Einheiten als Referenz ohne Verstärkung und drei mit Verstärkung getestet wurden. Es wurde eine spezielle Belastungseinrichtung im Labor konstruiert und hergestellt, so dass die Prüfstücke auf dem Boden stehen und seitliche zyklische Last, mit der Maßgabe einer vertikalen statischen Last, an den Proben angreifen. An allen Proben wurde eine extrem harte Belastungsgeschichte weggesteuert eingetragen, die in Übereinstimmung mit [ACI 374.1-05] aus progressiv ansteigenden Verschiebungsamplituden besteht, wobei drei Zyklen (Druck und Zug) auf

einem bestimmten Driftniveau liegen. Durch die experimentellen Untersuchungen bestätigt sich die exzellente Leistungsfähigkeit der verstärkten Probestücke sowie die Annahme, dass RT1 und RT2 in der Lage sind das Widerstandsvermögen mit einem Minimum an Festigkeits- und Steifigkeitsverlusten beizubehalten. Wie erwartet stieg die Kapazität zur Energiedissipation drastisch an und der „beam sidesway mechanism“ bildete sich tatsächlich aus.

Letztlich wurde die nichtlineare FE-Analyse durch Benutzung von ATENA alle verstärkten und nicht verstärkten Proben angewendet. Das FE-Modell wurde durch die experimentellen Ergebnisse validiert. Anschließend wurden die validierten Modelle benutzt, um eine neue vereinfachte Methode zur Verbesserung zu entwickeln, die auf den Vorzügen von RT1 und RT2 basieren. In der neu vorgeschlagenen innovativen Verstärkungstechnik 3 (RT3) wurde das HHDP durch eine Biegereibungsdämpferplatte (HFBDP) ersetzt, welche Energie basierend auf Reibung und Biegung dissipiert. Die Effektivität und Funktionsfähigkeit der vorgeschlagenen RT3 wurde mit Hilfe numerischer Analysen untersucht. Die Ergebnisse der Simulation zeigten, dass RT3 die Intention seismischer Verstärkung ebenfalls effizient erzielen könnte.

Letztlich, wie durch experimentelle und numerische Untersuchungen bestätigt, wird behauptet, dass alle geforderten Kriterien des ACI-Komitees [ACI 374.1-05] durch die vorgeschlagenen Verstärkungstechniken befriedigt wurden.

Schlagworte: Balken-Stützen-Verbindungen; Nachrüstung; Seismisch; Analyse; Konstruktion; Energiedissipation; Plastisches Gelenke; unelastische Verformung; Konsole; Reibung

Acknowledgments

First, and foremost, praises and thanks to the God, the Almighty, for providing me the blessings to complete this research successfully.

I wish to express my deep and sincere gratitude and appreciation to my research supervisors Prof. Dr.-Ing. Steffen Marx, Prof. Dr.-Ing. Nabil A. Fouad, and Prof. Dr.-Ing. Jürgen Grünberg for giving me the opportunity to develop this research and for providing me the guidance, encouragement and supporting throughout the course of this study that made this project possible.

I would like to appreciate Dr.-Ing. Michael Hansen for his supports during experimental study.

I would like to thank the all colleagues of Institute of Concrete Construction (IFMA), Leibniz University of Hannover, particularly Mrs. Kerstin Bensch, Mrs. Simone Matern and my dear friend Dipl.-Ing. Jens Piehler for their kindly assistance.

All experiments were conducted at structural laboratory of Institute of Concrete Construction (IFMA), Leibniz University of Hannover. I would like to show gratitude to technical staffs of the laboratory Mr. Ernst Heine and Mr. Olaf Menze for their distinguished assistance during the experimental study. I wish also to show appreciation to the other institutes' staff in the structural laboratory, Mr. Lothar Beer, Mr. Karl-Heinz Hentschel, Dipl. Ing. Christian Fricke, Mr. Viktor Wall, and Mr. Gerd Hargesheimer for their advices and assistance.

Materials (FRP composites, adhesives and SAS670 bolts) donated by FIDIA, Hardwire, Sika and Stahlwerk Annahute are thankfully acknowledged.

Last but not least, I wish to express my deep thankfulness to my family for their patience to wait in loneliness for the right time. Thanks to my lovely sons Amirhossein and Amirreza for their accompanying. My sincere gratitude to my wife Sonia for her supports, encouragements and patience during this study so that without her this work could not have been possible.

Table of contents

Abstract	i
Kurzzusammenfassung	iii
Acknowledgments	v
Table of contents	vi
List of figures	x
List of tables	xx
Notation	xxi
Chapter 1	1
Introduction	1
1.1 Introduction	1
1.2 Motivation of the research	4
1.3 Objectives	4
1.4 Organization of the research	5
Chapter 2	7
Background and State of the Art	7
2.1 Introduction	7
2.2 Seismic behaviour of substandard RC beam-column Joints	8
2.2.1 Summary of results	14
2.3 Retrofitting and strengthening techniques of beam-column joints	17
2.3.1 Epoxy repair procedures	17
2.3.2 Jacketing and other mechanical retrofitting techniques	22
2.3.3 Utilization of fiber-reinforced polymer composites, FRP	34
2.3.4 The summary of the results and discussion	51
2.4 Design approaches by codes of practice	54
2.4.1 The bond and shear requirements within the beam-column joints	54
2.4.2 Summary and conclusions of the codes comparison	57
Chapter 3	59
Seismic Retrofitting by Developing the Beam Sidesway Mechanism	59
3.1 Introduction	59
3.2 Seismic design principals of structures and joints	60
3.3 Performance-based retrofitting through developing the beam plastic hinges	63
3.3.1 Strategy of seismic retrofitting through the capacity design concept	63
3.3.2 Forces acting on an exterior beam-column joint	63
3.3.3 Strength and Failure Sequence Diagram (SFSD)	67
3.4 Innovative Multi Functional Corbels (HMFC)	70

3.4.1	General description	70
3.4.2	Hysteretic behaviour	72
3.5	Innovative Harmonica Damper Plates (HHDP)	77
3.5.1	General description	77
3.5.2	Hysteretic behaviour	78
3.6	An Innovative strengthening and retrofitting technique through Multi Functional Corbels (HMFC), Retrofitting Technique 1 (RT1)	82
3.6.1	Approach and modified SFSD	82
3.6.2	Upgrading the resistance to bond-slip of the beam bottom bars	86
3.6.3	Procedure for designing and developing	87
3.7	An Innovative strengthening and retrofitting technique through HMFC and Harmonica Damper Plates (HHDP), Retrofitting Technique 2 (RT2)	89
3.7.1	Approach and modified SFSD	89
3.7.2	Upgrading the resistance to bond-slip of the beam bottom bars	94
3.7.3	Procedure for designing and developing	94
Chapter 4	97
Experimental Program and Development	97
4.1	Introduction	97
4.2	Test specimens, energy dissipation devices and retrofitting	98
4.2.1	RC beam-column joint specimens	98
4.2.2	Multi Functional Corbels, HMFC	109
4.2.3	Harmonica Damper Plates, HHDP	116
4.2.4	Retrofitted specimens	120
4.3	Loading setup	141
4.3.1	General specifications	141
4.3.2	Details and fabrication of the loading setup	143
4.3.3	Testing procedure and loading history	143
4.4	Instrumentation	144
4.5	Experimental tests and results	150
4.5.1	Tests of reference units	151
4.5.2	Tests of retrofitted units	169
4.6	Test results and summary of findings	204
4.6.1	Strength	204
4.6.2	Energy dissipation	212
4.6.3	Damage mechanisms	216
4.6.4	Hierarchy of strength	217
4.6.5	Joint behaviour	218

4.6.6	Decomposition of lateral displacement	219
Chapter 5	221
Numerical Analysis and Simulations	221
5.1	Introduction	221
5.2	Implemented constitutive models in ATENA	222
5.2.1	Constitutive modelling of concrete	222
5.2.2	Constitutive modelling for reinforcement	228
5.2.3	Constitutive modelling for reinforcement bond	229
5.2.3	Constitutive modelling for Von Mises plasticity	229
5.2.4	Constitutive modelling for interface	229
5.3	Element types	230
5.4	Solutions of nonlinear equations	231
5.5	Numerical models for reference units	231
5.6	Sensitivity study	233
5.6.1	Sensitivity of element size	233
5.6.2	Sensitivity of fracture energy	234
5.6.3	Sensitivity of cyclic reinforcement	235
5.6.4	Sensitivity of tension stiffening	236
5.6.5	Sensitivity of cracking model	236
5.7	Numerical models for retrofitted specimens	237
5.8	Comparison the results of FE analysis and experimental test	241
5.8.1	Reference unit BD-B	241
5.8.2	Reference unit SD-B	243
5.8.3	Retrofitted specimen BD-H1	245
5.8.4	Retrofitted specimen SD-H2-D	248
5.8.5	Retrofitted specimen BD-H3-D	251
5.9	Developing a new upgrading method, Retrofitting Technique 3 (RT3)	254
Chapter 6	262
Conclusions and Recommendations	262
6.1	Conclusions	262
6.1.1	Conclusions of experimental study	262
6.1.2	Conclusions of numerical study	267
6.1.3	General conclusion	268
6.2	Recommendations for further research	269
References	270
Appendix A:	Supplementary Reviews of Laboratory Activities	279
Appendix B:	Scheme and Details of Loading Setup	282
Appendix C:	Installation of Specimens into the Loading Setup	305

Appendix D: Decomposition of Specimen Deformation	308
Appendix E: Concept of Relative Energy Dissipation Ratio	313

List of figures

Fig. 1.1: Global seismic hazard map produced by the Global Seismic Hazard Assessment Program(GSHAP 1999)	1
Fig. 1.2: Preliminary determination of Earthquake epicenters, 1963-1998(NASA, DTAM project team).....	1
Fig. 1.3: Population density (people per km ²) map of the world in 1994 (Wikipedia)	2
Fig. 1.4: Probabilistic Seismic hazard map for Germany, Austria, and Switzerland with map of epicenters, (Grüntal u.a. 1998).....	2
Fig. 1.5: Collapsed RC frame structure due to failure of beam-column joints, 1999, 7.2 Richter earthquake, Duzce, Turkey.....	3
Fig. 1.6: RC frame structure was collapsed via failure of beam-column joints, 1999, 7.4 Richter earthquake, Kocaeli, Turkey.....	3
Fig. 1.7: Joins failure leded to completely collapse of RC frame structure: a): 1994, Northridge earthquake, USA, 6.7 Richter (reprinted from [Moehle]); b) 20.04.2013, China's Sichuan province, 6.9 Richter, (Trend News).....	3
Fig. 2.1: Vacuum impregnation procedure [French et al.-90].....	18
Fig. 2.2: Masonry block jacketing technique [Bracci et al.-95-2].....	22
Fig. 2.3: Partial masonry infill technique [Bracci et al.-95-2]	23
Fig. 2.4: Prestressed concrete jacketing technique [Bracci et al.-95-2]	24
Fig. 2.4: Concrete jacketing technique [Alcocer -93] (reprinted from [Engindeniz et al.-05])	26
Fig. 2.5: a) Concrete jacketing using UNIDO strengthening technique; b) welding of new reinforcement to existing column reinforcement; c) details of steel collar stirrup. [Tsonos-99]	29
Fig. 2.4: Steel jacketing technique [Corazao -89] (reprinted from [Engindeniz et al.-05])	30
Fig. 2.5: Steel jacketing technique [Beres et al.-92] (reprinted from [Engindeniz et al.-05])..	31
Fig. 2.6: Corrugated Steel jacketing technique [Biddah et al.-97].....	32
Fig. 2.7: Planar joint expansion: a) Rectangular expansion, b) Triangular expansion [Chaimahawan-09]	34
Fig. 2.8: CFRP ductility and development retrofitting of beam-column join [Gen et al.-98]..	36
Fig. 2.9: a) Description of specimens and strengthening alternatives; b) layout of FRP layers [Antonopoulos -03]	38
Fig. 2.10: a) CFRP or GFRP strengthening; b) Strengthening of repaired specimens [Mukherjee-05].....	41
Fig. 2.11: Rehabilitation schemes [Ghobarah-05]	42
Fig. 2.12: Schematic representation of FRP repaired joint [Almusallam et al.-09].....	43
Fig. 2.13:a) FRP application details of specimens [Ilki et al.-11].....	44
Fig. 2.14: Typical rehabilitation schemes 1 and 2 [Li-11]	46
Fig. 2.15: Typical rehabilitation schemes: a) TR1; b) TR2 [El-Amoury-02]	47
Fig. 2.16: Typical rehabilitation schemes: a) T1R; b) T2R; c) T9 [Ghobarah-02]	49
(reprinted from[Said-04])	49
Fig. 2.17: GFRP retrofit configuration for the 3D corner joint specimen [Pampanin et al.-07]	50
Fig. 3.1: Global failure mechanisms of frame structures during a major earthquake	61

Fig. 3.2: Column sidesway mechanism led to 3 rd floor soft story collapse of reinforced concrete building in Nishinomiya, Kobe earthquake, Japan, 1995, Magnitude: 6.69 (Figure from USGS achieves)	61
Fig. 3.3: Retrofitting of the vulnerable existing frames by developing the beam plastic hinges	63
Fig. 3.4: Forces acting on an exterior beam-column joint.....	65
Fig. 3.5: Beam-column joint core stresses and the Mohr's circle	66
Fig. 3.6: Evaluation of hierarchy of strengths and sequence of events in M-N performance domain proposed by [Pampanin et al.-04]	68
Fig. 3.7: Proposed Strength and Failure Sequence Diagram (SFSD) in a beam-column joint in Vcol- N performance domain	69
Fig. 3.8: A sample of innovative Multi Functional Corbel (HMFC) with two pipes as energy dissipation element.....	71
Fig. 3.9: Different forms of Multi Functional Corbel (HMFC) and their FEM mesh patterns 73	
Fig. 3.10: Variations of hysteretic diagrams in six different variants of Multi Functional Corbels (HMFC)	74
Fig. 3.11: Relative lateral resistance and initial stiffness of different variants of Multi Functional Corbels (HMFC)	75
Fig. 3.12: Relative absorbed energy by different variants of Multi Functional Corbels (HMFC).....	76
Fig. 3.13: Comparison of a compression test and numerical analysis results on a pipe specimen of 10 mm length and internal diameter and thickness of 42 and 9.15 mm, respectively.....	76
Fig. 3.14: A sample of innovative Harmonica Damper Plate	77
Fig. 3.15: Instalation of innovative Harmonica Damper Plate (HHDP) into a pod	77
Fig. 3.16: Three different alternatives of innovative Harmonica Damper Plate	79
Fig. 3.17: Variations of hysteretic diagram in three different variants of innovative Harmonica Damper Plate (HHDP)	80
Fig. 3.17: Displacement-Stain diagrams of three different variants of innovative Harmonica Damper Plate (HHDP) for points 1 and 2	80
Fig. 3.18: Statically compression test of innovative Harmonica Damper Plate (HHDP)	81
Fig. 3.19: Finite element model of innovative Harmonica Damper Plate (HHDP)	81
Fig. 3.20: Experimental and numerical results of test and analysis of innovative Harmonica Damper Plate	81
Fig. 3.21: Internal forces in strengthened exterior beam-column joint with Multi Functional Corbel, Retrofitting Technique 1 (RT1).....	83
Fig. 3.22: The rehabilitation of development length of beam positive bars.....	86
Fig. 3.23: Internal forces in strengthened exterior beam-column joint with Multi Functional Corbel (HMFC) and Harmonica Damper Plates (HHDP), Retrofitting Technique 2 (RT2)	90
Fig. 3.24: Detail of H as referred to in Fig. 3.23 and assumed strain distribution in the strengthened beam section at the end of HMFC	92
Fig. 3.25: The rehabilitation of development length of beam positive bars.....	94
Fig 4.1: Test of concrete samples, tests of a) cubic compression, b) cylinder compression c) split, and d) modulus of elasticity	99

Fig. 4.2: The overall geometry of specimens	101
Fig. 4.3: Reinforcement details of specimens SD	102
Fig. 4.4: Reinforcement details of specimens BD	102
Fig. 4.5: Preparing of reinforcing bars	104
Fig. 4.6: Attaching strain gauges to reinforcing bars	105
Fig. 4.7: Production of reinforcement cages	106
Fig. 4.8: Production of formwork	106
Fig. 4.9: Wiring the strain gauges and temporary bracing the test specimens	107
Fig. 4.10: Casting of test specimens	108
Fig. 4.11: Curing the test specimens for at least one week	108
Fig. 4.12: Transferring the test specimens to depot and preserving them until the test time	109
Fig. 4.13: Dimensions and details of Multi Functional Corbel (HMFC) case H1	111
Fig. 4.14: Dimensions and details of Multi Functional Corbel (HMFC) case H2	111
Fig. 4.15: Dimensions and details of Multi Functional Corbel (HMFC) case H3	112
Fig. 4.16: Production process of Multi Functional Corbel (HMFC) case H1	114
Fig. 4.17: Production process of Multi Functional Corbel (HMFC) case H2	114
Fig. 4.18: Produced Multi Functional Corbel (HMFC) case H3	116
Fig. 4.19: Dimensions and details of Harmonica Damper Plate (HHDP) and its pod, D,	117
(First alternative)	117
Fig. 4.20: Dimensions and details of Harmonica Damper Plate (HHDP) and its pod, D', (Second alternative)	118
Fig. 4.21: Harmonica Damper Plate (HHDP): a) cutting the plate by water jet, b) HHDP ...	119
Fig. 4.22: Harmonica Damper Plate (HHDP) with its pod (case D) a) D set without lateral bracing of side pod arms, b) side view of D set, c) view of top side, d) view of bottom side	119
Fig. 4.23: Harmonica Damper Plate (HHDP) with its pod (case D') a) milling a slot into the connector plates by a universal milling machine , b) milled plates, c) components of D' set, d) connected D' set to the main test specimen and H3	120
Fig. 4.24: Expected Strength and Failure Sequence Diagram (SFSD) for as-built BD specimen	121
Fig. 4.25: Analysis of simplified structural retrofitted model BD-H1 under $V_{col} = 79.78$ kN ,	122
a) Moment diagram of structural model; b) The results of beam analysis	122
Fig. 4.26: Tension test of 3X2-12-12 Hardwire composite for 10 mm width	123
Fig. 4.27: Expected Strength and Failure Sequence Diagram (SFSD) for retrofitted specimen, BD-H1	125
Fig. 4.28: Retrofitting of the Bond Deficient specimen (BD) by Multi Functional Corbel (HMFC) H1 through RT1, (BD-H1)	126
Fig. 4.29: Details of connector components	128
Fig. 4.30: a) SAS 670/800-Stahlwerk Annahütte threaded steel bar with anchor nuts; b) Prepared angle connector (L1) with welded anchor nuts	129
Fig. 4.31: Application procedure of SRP 3X2-12-12 Hardwire sheet on the concrete for the shear strengthening of the specimen beam	131
Fig. 4.32: Retrofitted specimen BD-H1 placed in loading setup1H	131

Fig. 4.33: Expected Strength and Failure Sequence Diagram (SFSD) for as-built SD specimen	132
Fig. 4.34: Analysis of simplified structural retrofitted model SD-H2-D under Vcol = 95.74 kN , a) Moment diagram of structural model; b) The results of beam analysis	133
Fig. 4.35: Expected Strength and Failure Sequence Diagram (SFSD) for retrofitted specimen, SD-H2-D	135
Fig. 4.36: Retrofitting of the Shear Deficient specimen (SD) by Multi Functional Corbels (HMFC) H2 and Harmonica Damper Plates (HHDP) D through RT2, (SD-H2-D).....	136
Fig. 4.37: Retrofitted specimen SD-H2-D	137
Fig. 4.38: Analysis of simplified structural retrofitted model SD-H2-D under Vcol = 95.74 kN , a) Moment diagram of structural model; b) The results of beam analysis	138
Fig. 4.39: Retrofitting of the Bond Deficient specimen (BD) by Multi Functional Corbels (HMFC) H3 and Harmonica Damper Plates (HHDP) D' through RT2, (BD-H3-D)	140
Fig. 4.40: Retrofitted specimen BD-H3-D	141
Fig. 4.41: Designed loading setup	142
Fig. 4.42: Fabricated loading setup	142
Fig. 4.43: The applied cyclic drift history	143
Fig. 4.44: Location of load cells and Linear Variable Distance Transducers (LVDTs) for loading setup and as-built specimens (reference units).....	145
Fig. 4.45: Location of LVDTs for the retrofitted specimen BD-H1	146
Fig. 4.46: Location of LVDTs for the retrofitted specimen SD-H2-D	146
Fig. 4.47: Location of LVDTs for the retrofitted specimen BD-H3-D	147
Fig. 4.48: Location of strain gauges of reinforcing bars for the reference specimen.....	147
Fig. 4.49: Location of strain gauges of reinforcing bars for the retrofitted specimens:	148
a) for SD-H2-D, b) for BD-H1 and BD-H3-D	148
Fig. 4.50: Location of strain gauges of Multi Functional Corbels (HMFC) and threaded roads for the retrofitted specimen BD-H1	149
Fig. 4.51: Location of strain gauges of Multi Functional Corbels (HMFC), Harmonica Damper Plates (HHDP), and threaded roads for the retrofitted specimen SD-H2-D	149
Fig. 4.52: Location of strain gauges of Multi Functional Corbels (HMFC), Harmonica Damper Plates (HHDP), and threaded roads for the retrofitted specimen BD-H3-D	150
Fig. 4.53: Assumed signs of loading and displacement direction	151
Fig. 4.54: Final failure of specimen BD-B after the first cycle of 3.5% drift	152
Fig. 4.55: Experimental story shear-drift hysteretic response of specimen BD-B	152
Fig. 4.56: Imposed column axial load versus drift of specimen BD-B	153
Fig. 4.57: The envelope diagram for Max. strain of beam longitudinal bars at the beam- column interface versus story drift of specimen BD-B	153
Fig. 4.58: Crack patterns and damage mode sequence of specimen BD-B at different levels of drifts	156
Fig. 4.59: The relationship between joint principal tensile stress (f_{tj}^c) and story drift of specimen BD-B	157

Fig. 4.60: The relationship between absolute value of (joint horizontal shear stress) $ V_{jh}(A_e f_c) $ and story drift of specimen BD-B	158
Fig. 4.61: LVDT layout for measurement of joint shear deformation and horizontal displacement component	159
Fig. 4.62: The relationship among joint principal tensile stress ($f_{tj} f_c$), story drift, and joint shear deformation (γ) of specimen BD-B	159
Fig. 4.63: : Percentage contributions of beam, column and joint displacement in specimen BD-B to: a) total displacements in every drift level, b) total displacements of all drift levels.....	160
Fig. 4.64: Final failure of SD-B after 3.5% drifts level	161
Fig. 4.65: Experimental story shear-drift hysteretic response of specimen SD-B	162
Fig. 4.66: Imposed column axial load versus drift of specimen SD-B	162
Fig. 4.67: The envelope diagram for Max. strain of beam longitudinal bars at the beam-column interface versus story drift of specimen SD-B	163
Fig. 4.68: Crack patterns and damage mode sequence of specimen SD-B at different levels of drifts	165
Fig. 4.69: The relationship between joint principal tensile stress ($f_{tj} f_c$) and story drift of specimen SD-B.....	166
Fig. 4.70: The relationship between absolute value of (joint horizontal shear stress) $ V_{jh}(A_e f_c) $ and story drift of specimen SD-B	167
Fig. 4.71: The relationship among joint principal tensile stress ($f_{tj} f_c$), story drift, and joint shear deformation (γ) of specimen SD-B	167
Fig. 4.72: Percentage contributions of beam, column and joint displacement in specimen SD-B to: a) total displacements in every drift level, b) total displacements of all drift levels.....	168
Fig. 4.73: Retrofitted specimen BD-H1 after 4.5% drifts level	170
Fig. 4.74: Experimental story shear-drift hysteretic response of specimen BD-H1	170
Fig. 4.75: Imposed column axial load versus drift of specimen BD-H1	171
Fig. 4.76: The envelope diagram for Max. strain of beam longitudinal bars at the beam-column interface versus story drift of specimen BD-H1	172
Fig. 4.77: The envelope diagram for Max. strain of beam longitudinal bars at the end of HMFC versus story drift of specimen BD-H1	172
Fig. 4.78: Crack patterns and damage mode sequence of specimen BD-H1 at different levels of drifts	175
Fig. 4.79: The relationship between joint principal tensile stress ($f_{tj} f_c$) and story drift of specimen BD-H1	176
Fig. 4.80: The relationship between absolute value of (joint horizontal shear stress) $ V_{jh}(A_e f_c) $ and story drift of specimen BD-H1.....	177
Fig. 4.81: LVDT layout for measurement of joint shear deformation and horizontal displacement component of BD-H1	177
Fig. 4.82: The relationship among joint principal tensile stress ($f_{tj} f_c$), story drift, and joint shear deformation (γ) of specimen BD-H1	178
Fig. 4.83: The Hysteretic and envelope diagram for strain of top HMFC versus story drift of specimen BD-H1	179

Fig. 4.84: The Hysteretic and envelope diagram for strain of bottom HMFC versus story drift of specimen BD-H1	179
Fig. 4.85: Percentage contributions of beam, column and joint displacement in specimen BD-H1 to: a) total displacements in every drift level, b) total displacements of all drift levels.....	180
Fig. 4.86: Retrofitted specimen SD-H2-D after 4.5% drifts level.....	182
Fig. 4.87: Experimental story shear-drift hysteretic response of specimen SD-H2-D.....	182
Fig. 4.88: Imposed column axial load versus drift of specimen SD-H2-D.....	183
Fig. 4.89.: The envelope diagram for Max. strain of beam longitudinal bars at the beam-column interface versus story drift of specimen SD-H2-D.....	183
Fig. 4.90: The envelope diagram for Max. strain of beam longitudinal bars at the end of HMFC versus story drift of specimen SD-H2-D	184
Fig. 4.91: Crack patterns and damage mode sequence of specimen SD-H2-D at different levels of drifts	187
Fig. 4.92: The relationship between joint principal tensile stress (f_{tj}^c) and story drift of specimen SD-H2-D	187
Fig. 4.93: The relationship between absolute value of (joint horizontal shear stress) $ V_{jh}(A_e f^c) $ and story drift of specimen SD-H2-D.....	188
Fig. 4.94: LVDT layout for measurement of joint shear deformation and horizontal displacement component of SD-H2-D	189
Fig. 4.95: The relationship among joint principal tensile stress (f_{tj}^c), story drift, and joint shear deformation (γ) of specimen SD-H2-D	189
Fig. 4.96: The Hysteretic and envelope diagram for strain of top and bottom HMFCs versus story drift of specimen SD-H2-D	190
Fig. 4.97: The Hysteretic and envelope diagram for strain of top and bottom HHDPs versus story drift of specimen SD-H2-D	191
Fig. 4.98: Percentage contributions of beam, column and joint displacement in specimen SD-H2-D to: a) total displacements in every drift level, b) total displacements of all drift levels.....	192
Fig. 4.99: Retrofitted specimen BD-H3-D after 4.5% drifts level	194
Fig. 4.100: Experimental story shear-drift hysteretic response of specimen BD-H3-D	194
Fig. 4.101: Imposed column axial load versus drift of specimen BD-H3-D	195
Fig. 4.102.: The envelope diagram for Max. strain of beam longitudinal bars at the beam-column interface versus story drift of specimen SD-H2-D.....	195
Fig. 4.103: The envelope diagram for Max. strain of beam longitudinal bars at the end of HMFC versus story drift of specimen BD-H3-D	196
Fig. 4.104: Crack patterns and damage mode sequence of specimen BD-H3-D at different levels of drifts.....	199
Fig. 4.105: The relationship between joint principal tensile stress (f_{tj}^c) and story drift of specimen BD-H3-D.....	199
Fig. 4.106: The relationship between absolute value of (joint horizontal shear stress) $ V_{jh}(A_e f^c) $ and story drift of specimen BD-H3-D	200
Fig. 4.107: The relationship among joint principal tensile stress (f_{tj}^c), story drift, .. and joint shear deformation (γ) of specimen BD-H3-D.....	201

Fig. 4.108: The Hysteretic and envelope diagram for strain of top and bottom HMFCs versus story drift of specimen BD-H3-D.....	202
Fig. 4.109: The Hysteretic and envelope diagram for strain of top and bottom HHDPs versus story drift of specimen BD-H3-D.....	202
Fig. 4.110: Shear failure of bolts.....	203
Fig. 4.111: Percentage contributions of beam, column and joint displacement in specimen BD-H3-D to a) total displacements in every drift level, b)total displacements of all drift levels.....	204
Fig. 4.112: Comparison the hysteresis loops of as-built specimen BD-B with retrofitted unit BD-H1	206
Fig. 4.113: Comparison the hysteresis loops of as-built specimen BD-B with retrofitted unit BD-H3-D	206
Fig. 4.114: Comparison the envelop strengths in the category of BD	207
Fig. 4.115: Comparison the relative story shear strength in the negative and positive directions of the category of BD.....	208
Fig. 4.116: Comparison the hysteresis loops of as-built specimen SD-B with retrofitted unit SD-H2-D	209
Fig. 4.117: Comparison the envelop strengths in the category of SD.....	209
Fig. 4.118: Comparison the relative story shear strength in the negative and positive directions of the category of SD	210
Fig. 4.119: Comparison the envelop strengths of all specimens	210
Fig. 4.120: The retained column axial load at the end of last cycle of final drift level (3.5% for reference units and 4.5% for retrofitted specimens).....	211
Fig. 4.121: Comparison the maximum strength degradation of all specimens with respect to last cycle of 3.5% drift level.....	211
Fig. 4.122: Relatively comparison of initial stiffness in all specimens.....	212
Fig. 4.123: Comparison the energy dissipations in the category of BD.....	213
Fig. 4.124: Comparison the energy dissipations in the category of SD	213
Fig. 4.125: Comparison the energy dissipations in all specimens	214
Fig. 4.126: Comparison the energy dissipations in specimens and estimated contribution of subassemblages	215
Fig. 4.127: Comparison the energy dissipation ratio of retrofitted specimens in last cycle of 3.5% drift level.....	216
Fig. 4.128: Max. Observed joint horizontal shear stress in test specimens versus code-conforming nominal shear strength of the tested external joint.....	219
Fig. 4.129: Total percentage contributions of beam, column and joint displacement in every test specimen	220
Fig. 5.1: Uniaxial constitutive stress-strain law and softening law for concrete.....	223
Fig. 5.2: Definition of localization bands.....	224
Fig. 5.3: Biaxial failure function for concrete	226
Fig. 5.4: Rotated cracks and fixed crack regions	228
Fig. 5.5: Bilinear and multi-linear stress-strain law for reinforcement.....	228
Fig. 5.6: Failure surface for interface elements.....	230
Fig. 5.7: Typical interface model behaviour in: (a) shear, (b) tension.....	230
Fig. 5.8: Numerical model for: a) BD-B; b) SD-B.....	232

Fig. 5.9: Reinforcement model for: a) BD-B; and b) SD-B	233
Fig. 5.10: Envelope lateral strength-drift diagram for different FE element sizes.....	234
Fig. 5.11: Envelope lateral strength-drift diagram for various values of fracture energy (Gf)	235
Fig. 5.12: Envelope lateral strength-drift diagram for different reinforcement material	235
Fig. 5.13: Envelope lateral strength-drift diagram for various values of tension stiffening (Cts)	236
Fig. 5.14: Envelope lateral strength-drift diagram for different smeared cracking models ...	237
Fig. 5.15: Numerical model for BD-H1: a) General finite element mesh, b) Reinforcement, c) Multi Functional Corbel , HMFC (H1)	238
Fig. 5.16: Numerical model for SD-H2-D: a) General finite element mesh, b) Reinforcement.. c) Multi Functional Corbel HMFC (H2), d) Harmonica Damper Plate HHDP (D).....	239
Fig. 5.17: Numerical model for BD-H3-D: a) General finite element mesh, b) Reinforcement c) Multi Functional Corbel HMFC (H3), d) Harmonica Damper Plate HHDP (D')	240
Fig. 5.18: Story shear-drift hysteresis plot of reference unit BD-B from numerical analysis	241
Fig. 5.19: Envelope story shear-drift hysteresis plot of reference unit BD-B from numerical analysis and experimental study.....	242
Fig. 5.20: Overall final cracking pattern of reference unit BD-B	242
Fig. 5.21: Comparison of crack pattern for reference unit BD-B from: a) numerical analysis and b) experimental test	243
Fig. 5.22: Story shear-drift hysteresis plot of reference unit SD-B from numerical analysis	243
Fig. 5.23: Envelope story shear-drift hysteresis plot of reference unit SD-B from numerical analysis and experimental study.....	244
Fig. 5.24: Overall final cracking pattern of reference unit SD-B.....	244
Fig. 5.25: Comparison of crack pattern for reference unit SD-B from: a) numerical analysis and b) experimental test	245
Fig. 5.26: Story shear-drift hysteresis plot of retrofitted specimen BD-H1 from numerical analysis.....	245
Fig. 5.27: Envelope story shear-drift hysteresis plot of retrofitted specimen BD-H1 from numerical analysis and experimental study.....	246
Fig. 5.28: Comparison of crack pattern for retrofitted specimen BD-H1 from: a) numerical analysis and b) experimental test	247
Fig. 5.29: Principal yield strain pattern for HMFC (H1) in retrofitted specimen BD-H1	248
Fig. 5.30: Story shear-drift hysteresis plot of retrofitted specimen SD-H2-D from numerical analysis.....	248
Fig. 5.31: Envelope story shear-drift hysteresis plot of retrofitted specimen SD-H2-D from numerical analysis and experimental study.....	249
Fig. 5.32: Comparison of crack pattern for retrofitted specimen SD-H2-D from: a) numerical analysis and b) experimental test	250
Fig. 5.33: Principal yield strain pattern for HMFC (H2) in retrofitted specimen SD-H2-D..	250
Fig. 5.34: Principal yield strain pattern for HHDP (D) in retrofitted specimen SD-H2-D	251
Fig. 5.35: Story shear-drift hysteresis plot of retrofitted specimen BD-H3-D from numerical analysis.....	251
Fig. 5.36: Envelope story shear-drift hysteresis plot of retrofitted specimen BD-H3-D from numerical analysis and experimental study.....	252

Fig. 5.37: Comparison of crack pattern for retrofitted specimen BD-H3-D from: a) numerical analysis and b) experimental test	253
Fig. 5.38: Principal yield strain pattern for HMFC (H3) in retrofitted specimen BD-H3-D	253
Fig. 5.39: Principal yield strain pattern for HHDP (D') in retrofitted specimen BD-H3-D ..	254
Fig. 5.40: Retrofitting Technique 3 (RT3) by HMFC and HFBDP	255
Fig. 5.41: Friction test between steel plates and concrete surface: a) an innovative designed friction test device; b) fabricated test device; c) installation of test device in test machine	256
Fig. 5.42: Comparison of load-slip curves of steel-concrete friction in test and simulation: a) for grinded surface of concrete; b) for not grinded surface of concrete.....	256
Fig. 5.43: Crack pattern of developed new upgrading method, Retrofitting Technique 3 (RT3) for numerically analysed specimen BD-H1-F.....	257
Fig. 5.44: Story shear-drift hysteresis plot of developed new upgrading method, Retrofitting Technique 3 (RT3) for numerically analysed specimen BD-H1-F	258
Fig. 5.45: Envelope story shear-drift hysteresis plot of developed new upgrading method, Retrofitting Technique 3 (RT3) for numerically analysed specimen BD-H1-F	258
Fig. 5.46: Principal yield strain pattern for HMFC (H1) and HFBDP (F) in retrofitted specimen BD-H1-F	259
Fig. 5.47: Principal yield strain pattern for HFBDP (F) in retrofitted specimen BD-H1-F ...	259
Fig. 5.48: Comparison the energy dissipations in all specimens	260
Fig. 5.49: Comparison the energy dissipation ratio of retrofitted specimens in last cycle of 3.5% drift level	261
Fig. 5.50: Comparison the energy dissipations in specimens and estimated contribution of subassemblages	261
Fig. A.1: Formwork Plan.....	279
Fig. A.2: Details of formwork	280
Fig. A.3: a) Specimen bracing, b) Formwork and bracing.....	281
Fig. B.1: Designed loading setup	282
Fig. B.2: Fabricated loading setup	283
Fig. B.3: Loading setup: Top view of level 5.....	284
Fig. B.4: Loading setup: Top view of level 4.....	285
Fig. B.5: Loading setup: Top view of level 3.....	286
Fig. B.6: Loading setup: Top view of level 2.....	287
Fig. B.7: Loading setup: Top view of level 1	288
Fig. B.8: Loading setup: Details of top compartment (Det. 1).....	289
Fig. B.9: Loading setup: Fabricated top compartment.....	289
Fig. B.10: Loading setup: Checking the necessity of second mechanical hinge, balance case	290
Fig. B.11: Loading setup: Checking the necessity of second mechanical hinge, side sway to left.....	291
Fig. B.12: Loading setup: Checking the necessity of second mechanical hinge, side sway to right	291
Fig. B.13: Loading setup: Details of designed second mechanical hinge.....	292
Fig. B.14: Loading setup: Fabrication of second mechanical hinge	293
Fig. B.15: Loading setup: Second mechanical hinge, Max. allowable rotation.....	293

Fig. B.16: Loading setup: Rotation of second mechanical hinge.....	294
Fig. B.17: Loading setup: Details of top compartment (Det. 3).....	294
Fig. B.18: Loading setup: Details of movable support (Det. 4).....	295
Fig. B.19: Loading setup: Fabrication of movable support (Det. 4).....	296
Fig. B.20: Loading setup: Details of fixed hinge (Det. 5).....	297
Fig. B.21: Loading setup: Fabrication of fixed support (Det. 5).....	298
Fig. B.22: Loading setup: Details of reaction frame (Det. 6).....	299
Fig. B.23: Loading setup: Fabrication of reaction frame and its connection (Det. 6).....	301
Fig. B.24: Loading setup: Details of base plates (Det. 7).....	301
Fig. B.25: Loading setup: Fabricated base plate (Det. 7).....	302
Fig. B.26: Loading setup: Designed lateral support of test specimens.....	302
Fig. B.27: Loading setup: fabricated lateral support of test specimens.....	303
Fig. B.28: Loading setup: a) overhead horizontal traveling support of cyclic actuator, b) cyclic actuator.....	303
Fig. B.29: Loading setup: a) installation of cyclic actuator to loading setup, b) installed cyclic actuator.....	304
Fig. B.30: Loading setup: a) loading setup, b) hydraulic jack for static loads.....	304
Fig. C.1: Loading setup: Proposed installation process of specimens in loading setup.....	306
Fig. C.2: Loading setup: Installation of specimens in loading setup.....	307
Fig. D.1: Measurement of beam and column fix-end rotation.....	308
Fig. D.2: Measurement of joint deformation: a) LVDT layout for joint shear strain measurement, b) Sign conventions for joint shear strain.....	309
Fig. D.3: Contribution of beam, column and joint to the total lateral displacement.....	311
Fig. D.4: Measurement of beam rotation at the end of HMFC.....	311
Fig. D.5: Contribution of beam at the end of HMFC to the total lateral displacement.....	312
Fig. E.1: Concept of relative energy dissipation ratio.....	313

List of tables

Table 2.1: Comparison of the codes of practice in design of exterior beam-column joints.....	55
Table 4.1: Average measured properties of concrete	99
Table 4.2: Average measured properties of reinforcing steel bars.....	100
Table 4.3: Summary of the design requirements for the test specimens based on the codes of practice for seismic resistant	103
Table 4.4: Summary of the predicted nominal strengths of beam-column joint specimens' subassemblages	103
Table 4.5: Summary of the retrofitted specimen's nomination.....	110
Table 4.6: Properties of 3X2-12-12 Hardwire composite	123
Table 4.7: Failure modes of test specimens	216
Table 4.8: Hierarchy of strength for reference units	217
Table 4.9: Hierarchy of strength for retrofitted specimens	217
Table 4.10: Joint stresses and strains of test specimens	218

Notation

A_{ch}	cross-sectional area of a structural member measured to the outside edges of transverse reinforcement, mm^2
A_e	effective joint cross-sectional area, mm^2
A_g	gross area of concrete, mm^2
A_h	the area of the third cycle to the drift ratio of 3.5%
A_j	effective joint cross-sectional area, mm^2 , computed from joint depth (h_c) times effective joint width (the overall width of the column, except where a beam frames into a wider column, effective joint width shall not exceed the smaller of: a) beam width plus joint depth, b) twice the smaller perpendicular distance from longitudinal axis of beam to column side)
A_{s1}	area of the beam top reinforcement, mm^2
A_{s2}	area of the beam bottom reinforcement, mm^2
A_{sh}	total cross-sectional area of transverse reinforcement including crossies within spacing s and perpendicular to dimension b_c , mm^2
$A_{sv,i}$	total area of the intermediate bars placed in the relevant column faces between corners of the column including bars contributing to the longitudinal reinforcement of columns, mm^2
A_{Tjh}	total area of the horizontal hoops in a beam-column joint, mm^2
b_b	width of the longitudinal beam, mm
b_c	width of the column, mm
b_j	effective joint width, mm, should not exceed the smallest of $(\frac{b_b+b_c}{2}, b_b + \frac{\sum mh_c}{2}, b_c)$, where beam-column eccentricity exceeds $b_c/8$, $m=0.3$, otherwise $m=0.5$
b_{jj}	effective joint width, if $b_c > b_w$: $b_{jj} = \min\{b_c; (b_w + 0.5h_c)\}$; if $b_c < b_w$: $b_{jj} = \min\{b_w; (b_c + 0.5h_c)\}$
b_w	width of beam web, mm
d_b	nominal diameter of bar, mm
E_0	initial elastic modulus for concrete, MPa
E_c	secant elastic modulus at the peak stress for concrete, MPa
E_1	the peak lateral resistance for the positive lateral loading direction

E_2	the peak lateral resistance for the negative lateral loading direction
f_{cd}	design value of concrete compressive strength, MPa
F_{ps}	post-tensioning force of the bottom corbel, N
f'_c	specified compressive strength of concrete, MPa
$f_c^{'ef}$	concrete effective compressive strength, MPa
$f_t^{'ef}$	the effective tensile strength, MPa
f_{cd}	design value of concrete compressive strength, MPa
f_{ck}	strength of concrete, MPa
f_{ctd}	design value of the tensile strength of concrete, MPa
f_{ctm}	mean value of tensile strength of concrete, given as $0.3f_c^{(0.667)}$
f_y	specified yield strength of reinforcement, MPa
f_{yd}	design value of yield strength, MPa
f_{yt}	specified yield strength of transverse reinforcement, MPa
f_{ywd}	design value of the yield strength of the transverse reinforcement, MPa
h_c	overall cross-sectional depth of column, mm
h_{jc}	distance between extreme layers of column reinforcement, mm
h_{jw}	distance between the top and the bottom reinforcement of the beam, mm
h_v	vertical distance of horizontal LVDTs at the end of beam or HMFC, mm
h_h	horizontal distance of vertical LVDTs at the end of column, mm
h_x	Max. center-to-center spacing of crosstie legs on all faces of the column, mm
J_2	second invariant of stress deviator tensor
k	shape parameter the relation of Stress-strain for concrete
l_c	story height, length of column, measured center-to-center of the top and bottom beams, mm
l_{cn}	clear length of the column, mm
l_b	span length of beam, measured center-to-center of the column, mm
l_d	development length in tension of deformed bar based on the building codes, mm
l_{dh}	development length in tension of deformed bar with a standard hook, measured from critical section to outside end of hook, mm
l_{nb}	clear length of beam from face of columns, mm

M_{bc}	Joint moment at the beam joint interface, N.m
\bar{M}_{bc}	joint moment capacity of the exterior beam-column joint at the beam joint interface, N.m
M_{nbc}	beam bending moment capacity or beam yielding at joint interface, N.m
M_{ncb}	column bending moment capacity or column yielding at joint interface, N.m
N	column axial load, N
N_{Ed}	design axial force from the analysis for the seismic design (the minimum value from load combination), is assumed positive when compressive, N
s	center-to-center spacing of transverse reinforcement within the joint, mm
r_{ec}	reduction factor of the compressive strength
r_{et}	reduction factor of the tensile strength
V_b	shear force across the beam, N
V_c	shear force in the column above the joint, from the analysis in the seismic design situation, N
V_{col}	shear force in the column above the joint, N
\bar{V}_{col}	story shear capacity of the as-built exterior beam-column joint corresponding to the certain strength, N
$\bar{\bar{V}}_{col}$	story shear capacity of the retrofitted exterior beam-column joint corresponding to the certain strength, N
v_d	normalized design axial force of column
V_{jhd}	horizontal shear force acting on the concrete core of the exterior joint, N
V_{jh}	horizontal shear force acting on the concrete core of the exterior joint, N
V_{nb}	beam shear strength, N
V_{nc}	column shear strength, N
w	the crack opening, mm
w_c	crack opening at the complete release of stress, mm
x	normalized strain
Z_b	internal moment arm in the beam, mm
Z_{ps}	proper moment arm of the bottom corbel post-tensioning, mm
α	stress multiplier for beam longitudinal bars
β	relative energy dissipation ratio
γ	joint shear strain
γ_{Rd}	model uncertainty factor for the design value of resistance for beam

	longitudinal bars, given as 1.2
γ_{xz}	shear strain
ε	normal strain
ε_c	strain at the peak stress f_c^{ef}
ε_x	normal strain of joint panel in the x direction
ε_z	normal strain of joint panel in the z direction
ε_φ	strain in joint panel in an arbitrary direction (diagonal) with an angle of φ measured counter clockwise from the x axis
θ'_1	drift ratio in positive direction
θ'_2	drift ratio in negative direction
σ_c^{ef}	concrete compressive stress for the relation of Stress-strain for concrete, MPa
η	reduction factor on concrete compressive strength due to tensile strain in transverse direction
$\sum M_{nc}$	sum of nominal flexural strength of columns framing into the joint, N.mm
$\sum M_{nb}$	sum of nominal flexural strength of beams framing into the joint, N.mm
ACI	American Concrete Institute
ASCE	American Society of Civil Engineers
BD	Bond Deficiency
CFRP	Carbon Fiber-Reinforced Polymer
CORDIS	Community Research and Development Information Service
CSA	Canadian Concrete Design Code
DIN	Deutsches Institut für Normung
DTAM	Digital World Tectonic Activity Map
FRP	Fiber-Reinforced Polymer
EN	Europäische Norm
HFBDP	Hayatrouhi Frictional-Bending Damper Plate
HHDP	Hayatrouhi Harmonica Damper Plate
HMFC	Hayatrouhi Multi Functional Corbel

HPFRC	High-Performance Fiber-Reinforced Concrete
GFRP	Glass Fiber-Reinforced Polymer
GLD	Gravity Load Designed
GSHAP	Global Seismic Hazard Assessment Program
LVDT	Linear Variable Distance Transducer
NASA	National Aeronautics and Space Administration
NPO	Non Profit Organisationen
NSM	Near-Surface-Mounted
RC	Reinforced Concrete
RT1	Retrofitting Technique 1
RT2	Retrofitting Technique 2
RT3	Retrofitting Technique 3
SD	Shear Deficiency
SRP	Steel Fiber-Reinforced Polymer
SFSD	Strength and Failure Sequence Diagram
UNIDO	United Nations Industrial Development Organization
USGS	United States Geological Survey